Chemical Engineering Journal 431 (2022) 133388

Contents lists available at ScienceDirect

Chemical Engineering Journal

journal homepage: www.elsevier.com/locate/cej

Energy-balanced and effective adsorption-catalytic multilayer bed system for removal of volatile organic compounds

Sebastian Jarczewski [a], Katarzyna Barańska [a], Marek Drozdek [a], Marek Michalik [b], Katarzyna Bizon [c], Piotr Kuśtrowski [a,*]

[a] Department of Chemical Technology, Faculty of Chemistry, Jagiellonian University, Gronostajowa 2, 30-387 Kraków, Poland
[b] Institute of Geological Science, Faculty of Geography and Geology, Jagiellonian University, Gronostajowa 3a, 30-387 Kraków, Poland
[c] Faculty of Chemical Engineering and Technology, Cracow University of Technology, Warszawska 24, 31-155 Kraków, Poland

ARTICLE INFO

Keywords:
VOCs removal
Toluene
Adsorption
Catalytic combustion
Nanoreplication
Energy demand calculations

ABSTRACT

A dual-functional adsorption-catalytic system for elimination of volatile organic compounds (VOCs) in a cyclic mode, consisting of various configurations of three components, i.e. carbon adsorbent, inert silica separator and Pt/ZrO_2 catalyst, was developed. Both adsorbent and ZrO_2 support were synthesized by the nanoreplication method using spherical silica as a template, whereas the Pt active phase was deposited by the polyol approach. Properties of the functional materials were studied by several techniques, including N_2 adsorption, SEM-EDS, TGA, XRD, XRF and XPS. It was shown that the inert silica separator played an essential role protecting the carbon adsorbent from undesirable partial oxidation. The highest possible effectiveness of the toluene removal (conversion of 94.5%) was obtained for the configuration with 150 mg of Pt/ZrO_2 per 40 mg of the adsorbent. A fair stability of the optimal dual-functional system was proved by performing five consecutive adsorption–desorption-oxidation cycles. The experimental study was complemented by energy demand calculations, which confirmed the superiority of the hybrid system over a classic catalytic flow reactor in terms of energy requirements for the desorption-oxidation step. It was demonstrated that the system might operate autothermally due to a substantial amount of generated heat. Additionally, a simplified dynamic mathematical model of the system was developed, which enabled the identification of key aspects, including directions towards more complex mathematical description, to be taken into account in further research aimed at optimization of the hybrid system. The proposed hybrid dual-functional system can therefore be a step forward in developing cost-effective elimination technologies of VOCs from lean waste gases.

1. Introduction

Polluted air in urban areas can be harmful not only for human health, but also for plants and animals after a long-time exposure. Among different types of environmental hazards, the photochemical smog has been identified as a serious problem in last decades. The formation of this specific type of smog driven by ultraviolet radiation from the sunlight and accelerated by warm conditions of built-up cities is related to an increased emission of various pollutions due to industrialization and fast economic growth [1,2]. In contrast to a near-ground haze (commonly known as smog), a combination of smoke and fog, the essential constituents of detrimental photochemical smog are ozone (O_3) and peroxyacetyl nitrate (PAN) produced from directly emitted airborne species like NO_x and volatile organic compounds (VOCs) [3]. The latter includes dozens of chemicals belonging to different families (e.g. alkanes, alkenes, aromatic compounds, alcohols, aldehydes, ketones, halogenated hydrocarbons) and are massively used in various fields of industry. These substances are also often categorized as primary pollutants, because they can be toxic and carcinogenic themselves [4]. The annual non-methane volatile organic compound (NMVOCs) emission in the European Union countries (EU-28) was estimated to be 6,409 Gg in 2019 [5]. Despite the global VOCs emission from natural sources dominate over discharges from a variety of anthropogenic activities by a factor of ~10, the concentration of anthropogenic VOCs in urban areas is significantly higher [6,7].

In order to control the VOCs emission, diverse elimination techniques, including adsorption [8], membrane separation [9], biological treatment [10] and oxidation methods [11,12], have been developed. The adsorption with subsequent reuse of discharged VOCs as well as the

* Corresponding author.
E-mail address: piotr.kustrowski@uj.edu.pl (P. Kuśtrowski).

https://doi.org/10.1016/j.cej.2021.133388
Received 14 September 2021; Received in revised form 29 October 2021; Accepted 31 October 2021
Available online 6 November 2021

Nomenclature

AC	adsorption capacity of a particular adsorbent-catalyst system towards toluene, mmol/g
$c_{p,i}$	specific heat capacity of a solid component i, J/(kg·K)
$C_{p,i}$	isobaric heat capacity of a gas component i, J/(mol·K)
C_{VOC}	molar concentration of VOC in a gas phase, mol/m^3
d_{in}	reactor inner diameter, mm
d_{out}	reactor outer diameter, mm
ΔH_{des}	heat of desorption, J/mol
ΔH_{reac}	heat of reaction, J/mol
k_{app}	apparent rate constant of a chemical reaction, 1/s
m_i	mass of a component i, kg
n_i	number of moles of a component i, mol
$\dot{n}_{i,j}$	molar flow rate of a component i in layer j of a reactor, mol/s
NC	non-combusted toluene, mmol
PC	performance coefficient, mmol/cycle
q	concentration of adsorbed molecules, mol/kg
q_{AC}	specific adsorption capacity of C_SPH, mol/kg
Q	heat, J
r_{VOC}	reaction rate per unit volume of a reactor, mol/m^3
t	time, s
T	temperature, K
V_i	total volume (including voids) of a layer i of the reactor, m^3
X_{voc}	toluene conversion degree
y_i	molar fraction of a component i
ε_b	bed porosity
$\varepsilon_{p,i}$	particle porosity made of material i
$\rho_{app,j}$	apparent density of material i, kg/m^3

thermal total oxidation of VOCs are the two most promising solutions for purification of polluted air streams where the concentration of VOCs is relatively high. However, the treatment of low-concentrated waste gases by these methods is unprofitable. Hence, highly diluted VOCs are emitted into the atmosphere, contributing to the formation of photochemical smog in the same way as those released from more concentrated sources.

To enable cost-effective elimination of VOCs from lean waste gases, the application of hybrid method coupling adsorption, subsequent desorption, and finally catalytic combustion of condensed stream of organic pollutants can be applied. In the literature some systems containing one specific material, which acts as both adsorbent and catalyst, have been described [13–22]. Recently, Adebayo et al. constructed hybrid systems for simultaneous adsorption and oxidation of VOCs on $TiO_2(ZrO_2)/SiO_2$ [23], Ni/ZrO_2-SiO_2 [24] and $Pd(TiO_2)$/MIL-101 [25]. In the elimination of toluene and benzene (used as model VOCs representatives) encouraging conversions of 71–86% were achieved. However, such approach seems to be a kind of compromise, because the developed material must exhibit sufficient performance in both processes (adsorption and catalytic oxidation), which are quite different in their nature. Consequently, the overall effectiveness of a one-component dual-functional system would be limited. Moreover, up to date the combined adsorption-catalytic processes have been examined mostly in continuous flow converters. We suppose that a more reliable strategy is based on combining two suitable materials working effectively in the specific process (one would be responsible solely for adsorption while another one for catalytic combustion of VOCs). The beneficial effectiveness of this kind of dual-functional system is based on the principle of operation, where adsorption of VOCs takes place without energy demand. This stage is the longest one, especially when lean waste gases are purified. In consequence, the heat necessary for catalytic oxidation is required only for the relatively short time of VOCs desorption and combustion. Such hybrid adsorption-catalytic systems have been scarcely described in scientific literature. In the recent study, Xie et al. [26] reported a promising dual-functional system, in which the modified carbon fibers were used as an adsorbent and a Pt/Ni material as a total oxidation catalyst. Adsorption of VOCs followed by their combustion was also studied on different materials by Kullavanijaya and co-workers [27], but the information provided is rather scant. An interesting study was shown by Guillemot et al. [28] who carried out the adsorption/catalysis process on modified faujasite zeolites using two separate materials beds and a movable furnace. Nevertheless, kinetics of the entire process was not controlled. On the other hand, an analysis of energy efficiency for dual-functional adsorption-catalytic systems is limited. Atwood et al. [20] compared the energy demand for hybrid and classic combustion-based systems. However, they considered only simple time differences and energy required to raise temperature in a feed stream from ambient to reaction temperature.

In the presented study we discuss physicochemical features of a sucrose-derived carbon adsorbent and a Pt-ZrO_2 catalyst, both synthesized by the nanoreplication technique using the same silica gel template in order to provide comparable morphology of the components adsorbent and catalyst beds. The synthesized materials were investigated in a hybrid adsorption-catalytic system for toluene removal at different conditions. We validated hypothesis regarding a positive energetic effect of the hybrid adsorption-catalytic system, and we distinguished crucial parameters responsible for the efficient toluene removal. In the calculations, which complement the performed experiments, the heat necessary to increase temperature of all components and the enthalpy of reaction is taken into account. In addition to the calculations focused on determining the energy demand, a simplified model of the hybrid system dynamics was formulated. To the best of our knowledge, such a comprehensive insight into the design and operation of the combined adsorption-catalytic system for the removal of VOCs using very active functional materials has not yet been presented and confirms the utility of this solution on a commercial scale.

2. Materials and methods

2.1. Synthesis of materials

A carbon adsorbent was synthesized using the incipient wetness impregnation technique. In a typical procedure, 1.00 g of a spherical silica gel template (fraction 40–75 μm, Supelco) was initially dried at 120 °C for 1 h and impregnated with a solution containing 0.77 g of deionized water, 0.19 g of sucrose (POCH) and 0.022 g of sulfuric acid (95–97%, Sigma-Aldrich). The obtained composite was placed in an oven at 100 °C for 6 h. Subsequently, the temperature was raised to 160 °C and the sample was kept at this temperature for the next 6 h. The procedure of impregnation and heating was repeated once, with a solution containing 0.64 g of H_2O, 0.16 g of sucrose and 0.018 g of H_2SO_4. Then, 1.20 g of the composite was carbonized in a N_2 environment (flow rate = 35 cm^3/min) in a tubular furnace at 800 °C for 4 h (heating rate = 1 °C/min). In the final step, the SiO_2 template was removed by dissolution in a 10% hydrofluoric acid solution at room temperature for 1 h. The obtained carbon replica was filtered, washed with 500 cm^3 of deionized water and 50 cm^3 of ethyl alcohol (96%, Avantor) and dried at room temperature overnight. The procedure of silica dissolution was repeated once. The spherical silica and the obtained carbon replica are denoted as SPH and C_SPH, respectively.

In the preparation of a zirconium oxide support, the incipient wetness impregnation method was used. Firstly, 45.0 g of spherical silica gel (fraction 40–75 μm, Supelco) after drying at 120 °C for 1 h was impregnated with an aqueous solution containing 45.0 g of $ZrOCl_2{\cdot}8H_2O$

(≥99.5%, Sigma-Aldrich) in 30.0 g of deionized water. The sample was dried at 90 °C for 24 h and calcined in a muffle furnace in air at 900 °C for 2 h (heating rate = 2 °C/min). The silica template was etched by a NaOH solution (3.0 mol/dm^3) in a polypropylene bottle at 50 °C for 24 h (20.0 cm^3 for 1 g of the composite). Finally, the resulting ZrO_2 replica was filtered, washed copiously with deionized water and dried at 90 °C for 24 h.

Platinum nanoparticles were deposited on the synthesized ZrO_2 support by a polyol process. Briefly, 0.0224 g of NaOH (p.a., POCH) was dissolved in 7.0 cm^3 of ethylene glycol (99%, anhydrous, J.T. Baker) in a round-bottom three-neck flask (25 cm^3) equipped with a reflux condenser and placed on a magnetic stirrer in an oil bath. Subsequently, 0.0468 cm^3 of $PtCl_4$ (96%, Sigma-Aldrich) was added and the suspension was stirred vigorously for 10 min. After the metal salt dissolution, the temperature was increased to 160 °C and maintained for 3 h. After cooling down, the brown solution containing colloidal Pt was deposited onto the ZrO_2 surface to obtain 1 wt% Pt loading in the final catalyst. The doped sample was mixed carefully, dried at 50 °C overnight, then washed copiously with deionized water and dried again at 70 °C. Finally, the material was ground in a mortar and calcined in air at 400 °C for 2 h (heating rate = 5 °C/min). The obtained supported catalyst is denoted as Zr_Pt.

2.2. Characterization of materials

Thermogravimetric analysis (TG) was performed with an SDT Q600 thermobalance (TA Instruments) in flowing air (100 cm^3/min) from 30 °C to 1000 °C (heating rate = 20 °C/min).

Powder X-ray diffraction (XRD) pattern of the Zr_Pt catalyst was collected with a Bruker D2 Phaser instrument using a Cu Kα radiation (λ = 1.54184 Å) and a LYNXEYE detector in the 2θ range from 15.0 to 70.0° with the step of 0.02° and 1 s or 5 s counting times per step.

Textural properties were determined on the basis of low-temperature nitrogen adsorption–desorption isotherms collected at −196 °C using a Micromeritics ASAP 2020 sorptometer. Prior to each measurement, a sample was degassed under vacuum (10^{-3} Pa) at 250 °C for 6 h. Specific surface areas (S_{BET}) were calculated using the Brunauer–Emmett–Teller model (BET). Values of total pore volume (V_{total}) were obtained from amounts of N_2 adsorbed at relative pressure $p/p_0 \sim 0.97$. Volumes of micropores (V_{micro}) were calculated using the t-plot method. Pore size distribution (PSD) was calculated with the equilibrium model of non-local density functional theory (NLDFT).

Quantitative analysis of the Pt active phase and Si residuals in the Zr_Pt catalyst was done by X-ray fluorescence spectroscopy (XRF) using a Thermo Scientific ARL Quant'x spectrometer.

X-ray photoelectron spectroscopy (XPS) was used to determine the surface composition of the Zr_Pt sample. The XPS spectra were collected in a Prevac photoelectron spectrometer equipped with a monochromatized aluminum source Al Kα (E = 1486.6 eV), a hemispherical analyzer (VG SCIENTA R3000) and a low energy electron flood gun (FS40A-PS) to compensate a charge of the nonconductive sample. Base pressure in the analytical chamber was 5×10^{-9} mbar. Areas and binding energies of Pt 4f, Zr 3d, Si 2p, Na 1s and C 1s photoelectron peaks were used to evaluate the chemical state of the surface. The deconvolution of the spectra was performed with the Shirley background model using CasaXPS software.

A field emission scanning electron microscope (Hitachi S-4700, Tokyo, Japan) equipped with an X-ray energy dispersive spectrometer (NORAN 7 with NSS Spectral Imaging System, Thermo Scientific, USA) was used for imaging and determination of distribution of elements (elemental mapping). For imaging, samples were mounted on carbon adhesive discs and coated with gold. A secondary electrons (SE) signal was used for observations at an accelerating voltage of 20 kV. The elemental mapping was performed on carbon coated samples. K-line for O and L-lines for both Zr and Pt were selected for the analyses. The acquisition time was selected experimentally.

2.3. Adsorption-catalytic tests

Adsorption of toluene, subsequent desorption and following catalytic combustion tests were carried out in a tubular flow quartz microreactor (8 mm i.d.) containing a multilayer bed consisting of various arrangement and volumes of the adjacent C_SPH adsorbent, inert SPH silica separator and Zr_Pt catalyst, all placed on a quartz wool plug. The configuration of the adsorption-catalytic system is schematically shown in Fig. 1. Gaseous reactants were fed through thermal mass flow controllers (Brooks SLA5800) from the top of the reactor. Temperature was measured with a thermocouple, protected by a quartz capillary inserted directly into the top layer (C_SPH). Toluene vapour was introduced into a flow of synthetic air (20% O_2/80% N_2, 6.0, Air Products) by passing it through a glass scrubber filled with a liquid toluene kept at −8.0 °C in a thermostatic bath. In a typical procedure, the adsorption-catalytic test consisted of four consecutive steps: (i) adsorption of the pollutant molecules on the surface of the C_SPH adsorbent performed in air saturated with toluene (40 °C, 100 cm^3/min), (ii) desorption of physisorbed forms of toluene by passing of pure air (40 °C, 100 cm^3/min), (iii) desorption of chemically adsorbed forms of toluene by flash heating to 250 °C (at the air flow stopped), and (iv) catalytic oxidation of desorbed toluene molecules in air (250 °C, 10 cm^3/min). Prior to the adsorption step, the materials were outgassed in nitrogen (5.2, Air Products) at 275 °C for 20 min. The temperature and time profile of the typical adsorption-catalytic experiment is depicted in Fig. 2. All products were continuously analysed with a quadrupole mass spectrometer (PREVAC UMS) connected on-line by a capillary to the reactor outlet. The adsorption capacity of toluene was determined with the same procedure as described above for the adsorption-catalytic tests, but performed entirely in inert environment (flowing N_2). The catalytic performance was evaluated in terms of toluene conversion (X_{VOC}) and performance coefficient (*PC*) defined as follows:

$$X_{VOC} = ((AC - NC)/AC) \times 100\% \quad (1)$$

$$PC = AC \times X_{VOC}[\text{mmol/cycle}] \quad (2)$$

where *AC* – adsorption capacity of a particular adsorbent-catalyst system towards toluene (chemically or physically adsorbed); *NC* – non-combusted toluene.

The Zr_Pt catalyst was also tested individually in the total oxidation of toluene at various temperatures. The catalytic test was carried out for 100 mg of the sample in the temperature range of 125–350 °C with the step of 25 °C (heating rate = 5 °C/min). The vapor concentration of toluene in flowing air (100 cm^3/min) was equal to 1000 ppm. Prior to the catalytic run, the sample was outgassed in an air stream (100 cm^3/min) at 350 °C for 30 min.

2.4. Calculation of energy requirement

The performance of the multilayer bed consisting of various arrangements and volumes of C_SPH, SPH and Zr_Pt was evaluated in terms of energy consumption during the process. The results were compared with those obtained for a competing system, i.e. a catalytic flow reactor. In both cases no heat losses were assumed. The calculations were carried out for the actual process occurring at 250 °C. Thus, initially, the temperature of the solids (i.e. reactor walls and bed particles) and adsorbate (in the case of the multilayer bed) needs to be increased from the ambient temperature to the process temperature. The amount of heat consumed for the system preheating was evaluated as:

$$Q_{preheat} = \sum m_i c_{p,i} (T_{proc} - T_{amb}) \quad (3)$$

where $c_{p,i}$ – specific heat capacity of a solid component *i*, m_i – mass of a component *i*, T_{amb} and T_{proc} – ambient and process operation temperature, respectively.

The energy supplied to preheat gas introduced into the reactor from

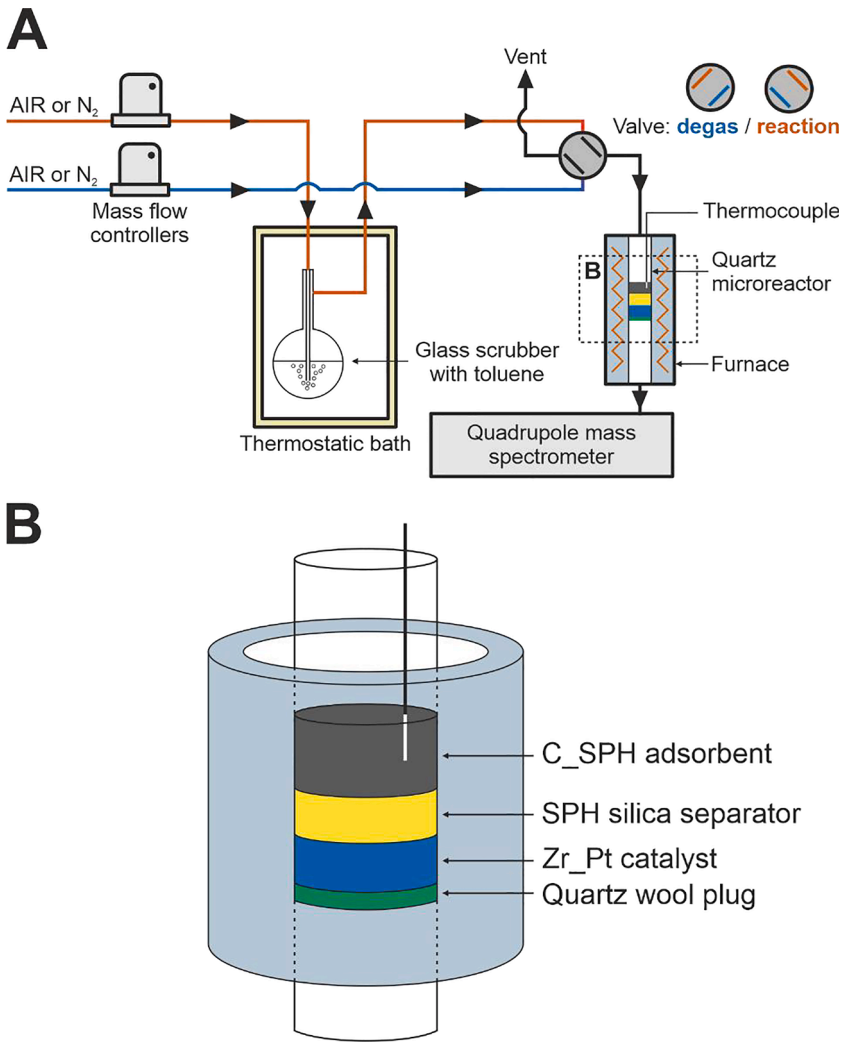

Fig. 1. Scheme of the adsorption-catalytic system (A) and enlarged fragment of multilayer bed configuration (B).

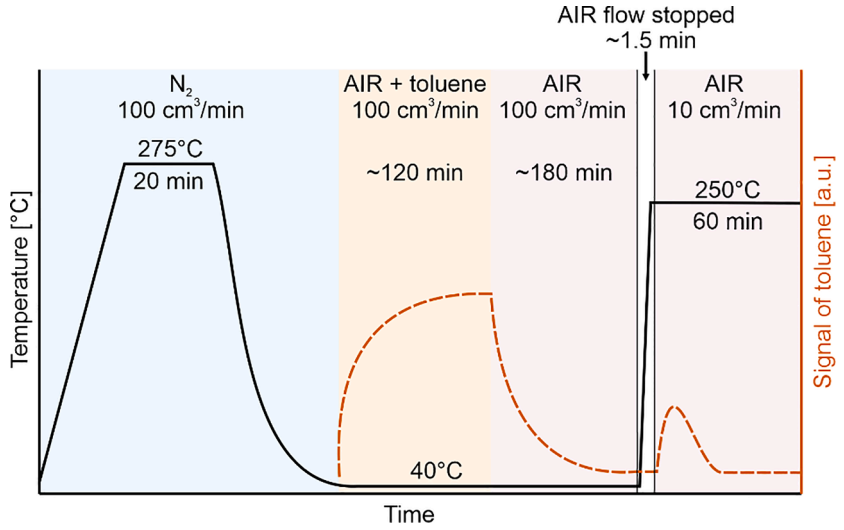

Fig. 2. Temperature and time profile of typical adsorption-catalytic experiment.

T_{amb} to T_{proc}, which depends on the process duration, gas composition and volumetric flow rate, was evaluated as:

$$Q_{gas} = \sum n_i C_{p,i}(T_{proc} - T_{amb}) \tag{4}$$

where $C_{p,i}$ – isobaric heat capacity of a component i, n_i – number of moles of a component i fed to the reactor within entire duration of the process.

For the adsorption-catalytic system operated with flowing air at the volumetric flow rate of 10 cm^3/min, the duration of the process was estimated based on the kinetics of desorption of toluene from C_SPH performed in the N_2 environment at 250 °C. The energetic performance of the catalytic flow reactor (with the bed containing Zr_Pt only) was evaluated based on the conditions used during the catalytic tests, i.e. for the stream of air saturated with 1000 ppm of toluene and supplied at the rate of 100 cm^3/min. The duration of the process was assumed to be equal to the time necessary to supply the conventional reactor with the same amount of toluene that is adsorbed on C_SPH in the corresponding adsorption-catalytic system.

For the multilayer bed, considering endothermic character of the desorption process, it is also necessary to account for the contribution of total heat of desorption, expressed here as:

$$Q_{des} = n_{\mathrm{VOC}} \Delta H_{ads} \tag{5}$$

where n_{VOC} – number moles of adsorbed toluene.

The above energy inputs to the system are balanced by the heat released during the toluene combustion:

$$Q_{reac} = X_{\mathrm{VOC}} n_{\mathrm{VOC}} \Delta H_{reac} \tag{6}$$

The net energy consumption for the flow reactor and adsorption-catalytic system was calculated as:

$$Q_{net,flow} = Q_{preheat} + Q_{gas} + Q_{reac} \tag{7}$$

$$Q_{net,ads\_cat} = Q_{preheat} + Q_{gas} + Q_{des} + Q_{reac} \tag{8}$$

2.5. Mathematical model

To better understand the behavior of the studied multilayer bed, a simplified dynamic model of the adsorption-catalytic system was formulated. The proposed model was based on the following assumptions: (i) the entire adsorption-catalytic system operates under isothermal conditions, (ii) pressure drop across the bed is neglected, (iii) gas-to-particle and intraparticle mass transport resistances are negligible, and (iv) gas is perfectly mixed within each layer of the bed. Small particle sizes, a very low length-to-diameter ratio of the operating bed and relatively low gas flow rates justify the mentioned simplification made within the model.

Given the above assumptions, the toluene mass balance in the adsorption-catalytic system was described by the following equations:

$$\left[\varepsilon_b + (1-\varepsilon_b)\varepsilon_{p,1}\right] \frac{dn_{\mathrm{VOC},1}}{dt} = \dot{n}_{\mathrm{VOC},in} - \dot{n}_{\mathrm{VOC},1} - (1-\varepsilon_b)\rho_{app,1}\frac{dq}{dt}V_1 \tag{9}$$

$$\left[\varepsilon_b + (1-\varepsilon_b)\varepsilon_{p,2}\right] \frac{dn_{\mathrm{VOC},2}}{dt} = \dot{n}_{\mathrm{VOC},1} - \dot{n}_{\mathrm{VOC},2} \tag{10}$$

$$\left[\varepsilon_b + (1-\varepsilon_b)\varepsilon_{p,3}\right] \frac{dn_{\mathrm{VOC},3}}{dt} = \dot{n}_{\mathrm{VOC},2} - \dot{n}_{\mathrm{VOC},3} - r_{\mathrm{VOC},3}V_3 \tag{11}$$

where ε_b – bed porosity, $\varepsilon_{p,i}$ – particle porosity (1 – C_SPH, 2 – SPH, 3 – Zr_Pt), $n_{\mathrm{VOC},i}$ – number of moles of toluene in a layer i, $\dot{n}_{\mathrm{VOC},i}$ - molar flow rate of toluene, V_i – total (i.e. including voids) volume of a layer i, $\rho_{app,1}$ – apparent density of C_SPH, q – concentration of adsorbed toluene, $r_{\mathrm{VOC},3}$ – toluene combustion rate per unit reactor volume. The inlet and initial conditions associated with the above equations are:

$$\begin{aligned} &\dot{n}_{\mathrm{VOC},in}(t) = 0 \\ &n_{\mathrm{VOC},1}(0) = n_{\mathrm{VOC},0} \\ &n_{\mathrm{VOC},2}(0) = n_{\mathrm{VOC},3}(0) = 0 \end{aligned} \tag{12}$$

The toluene balance equation in the third layer (Eq. (11)) is valid also for the conventional catalytic flow reactor. Considering steady-state operation mode of the conventional system, the balance equation for the Zr_Pt bed can be described as follows:

$$0 = \dot{n}_{\mathrm{VOC},2} - \dot{n}_{\mathrm{VOC},3} - r_{\mathrm{VOC},3}V_3 \tag{13}$$

The rate of desorption dq/dt in Eq. (9) was described using lognormal distribution approximation [29] of the experimental data collected during the desorption tests at 250 °C using pure N_2 as a purge gas. The instantaneous amount of the adsorbed toluene per unit adsorbent mass was thus expressed as:

$$q(t) = q_{AC} - q_{AC}\left[\frac{1}{2} + \frac{1}{2}\mathrm{erf}\left(\frac{lnt - \mu}{\sqrt{2}\,\sigma^2}\right)\right] \tag{14}$$

where q_{AC} – specific adsorption capacity of C_SPH, μ and σ – adjustable model parameters determined by the least square method.

For the conventional system, due to the presence of excess air, a simple first-order kinetic model (with respect to toluene) may be used to describe the oxidation rate r_{VOC} [30]. More complex rate formula, accounting for the oxygen consumption might be necessary for the adsorptive system. One possibility is the following kinetic model [31]:

$$r_{\mathrm{VOC}} = \frac{k p_{\mathrm{VOC}} p_{\mathrm{O_2}}}{(1/K_{\mathrm{VOC}} + p_{\mathrm{VOC}})(1/K_{\mathrm{O_2}} + p_{\mathrm{O_2}})} \tag{15}$$

3. Results and discussion

3.1. Physicochemical properties of adsorption-catalytic system components

The thermogravimetric measurement in air was performed to examine possible residues of SiO_2 in the structure of the C_SPH replica after the HF treatment in the last step of the synthesis. The registered curve is presented in Fig. 3. In the temperature range of 500–650 °C a steep loss of sample weight is observed as a result of carbon oxidation. The achieved weight loss of 100% clearly confirms that dissolving of the silica template was complete.

Table 1 presents calculated textural parameters of all the synthetized materials. Specific surface area of the spherical silica gel template is relatively high (S_{BET} = 294 m^2/g), however significantly lower than determined for the C_SPH carbon replica (S_{BET} = 1318 m^2/g). Such high

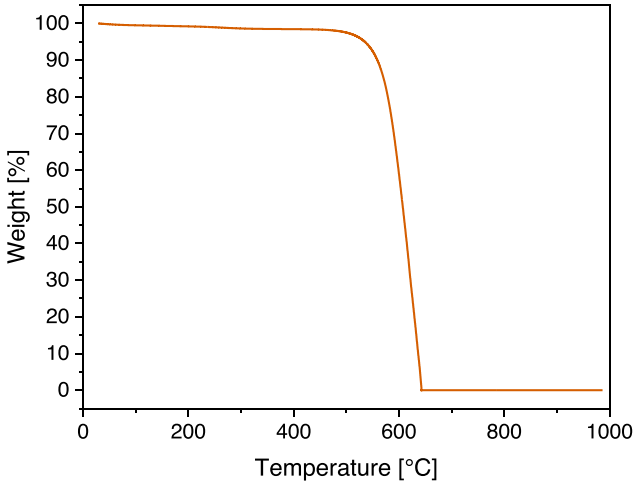

Fig. 3. Thermogravimetric curve of the C_SPH carbon replica registered in air.

Table 1
Textural properties and adsorption capacity of toluene for the SPH, C_SPH and Zr_Pt samples.

Sample	S_{BET} [m^2/g]	V_{total} [cm^3/g]	V_{micro} [cm^3/g]	Adsorption capacity of toluene [mmol/g]
SPH	294	0.83	0.03	0.00
C_SPH	1318	2.92	0.15	8.31
Zr_Pt	104	0.16	0.00	0.00

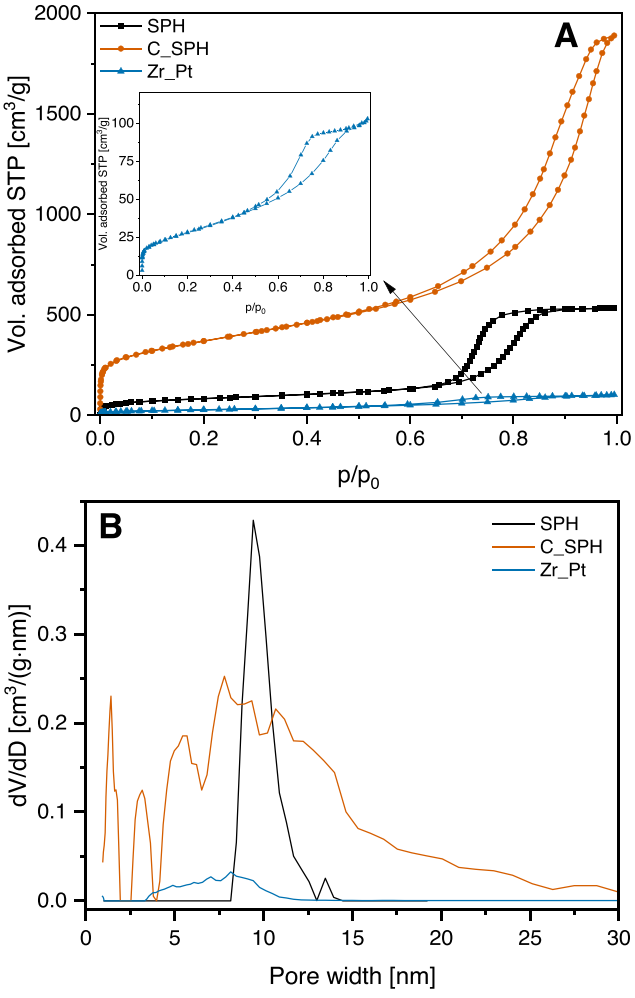

Fig. 4. Low-temperature nitrogen adsorption–desorption isotherms (A) and calculated pore size distributions (B) for the SPH, C_SPH and Zr_Pt samples.

surface area as well as total pore volume of C_SPH originate from microporosity created inside of the carbon rods by the liberation of gaseous products during the carbonization process. The presence of these additional micropores was confirmed by the t-plot calculations – an evident difference in the volume of micropores for SPH and C_SPH can be seen (cf. Table 1). Fig. 4A depicts low-temperature nitrogen adsorption–desorption isotherms collected for all the samples. In the case of the carbon replica, at a low relative pressure ($p/p_0 < 0.05$) a much higher amount of nitrogen is adsorbed compared to SPH, which corroborates the presence of higher contribution of micropores. The surface area of the Zr_Pt sample is significantly lower ($S_{BET} = 104$ m^2/g) in comparison to C_SPH, despite the same general synthesis strategy based on the SPH silica template. In this case, no additional porosity could be generated inside the ZrO_2 oxide structure, because of its chemical nature and progressive crystallization process. The incorporation of Pt species can additionally promote a decrease in the S_{BET} value as well as depletion of the hysteresis loop (cf. inset of Fig. 4A). According to IUPAC Technical Report, all the measured isotherms can be assigned to type IV(a) typical of mesoporous materials, where adsorption is similar as for type II, but followed by pore condensation with a hysteresis loop (type H2(b)) and final saturation plateau [32]. The characteristic feature of type H2(b) hysteresis loop is a gentle desorption branch attributed to blocking of pore necks with a quite broad size distribution. Pore size distribution of the SPH sample (Fig. 4B) shows narrow maximum at ca. 9 nm, confirming mesoporosity of the SiO_2 separator. No additional pores are observed in contrast with the C_SPH sample, where both micro- and mesopores are found. However, the peak related to mesopores is much wider than in SPH, indicating broad range of mesopore diameters in the carbon sample. Such broadening is related with the fact that carbon replica is a negative of the SPH template and porosity originates from dissolution of silica walls of SPH. Micropores of the C_SPH sample were generated mostly inside the carbon walls of the material during the carbonization process. The PSD of the Zr_Pt catalyst shows relatively small peak at ca. 6 nm, which confirms mesoporosity and its low total pore volume (cf. Table 1), estimated earlier from the isotherm.

The X-ray diffraction pattern of the Zr_Pt sample is presented in Fig. 5A. The diffraction peaks can be identified at 31.0°, 35.0°, 51.0° and

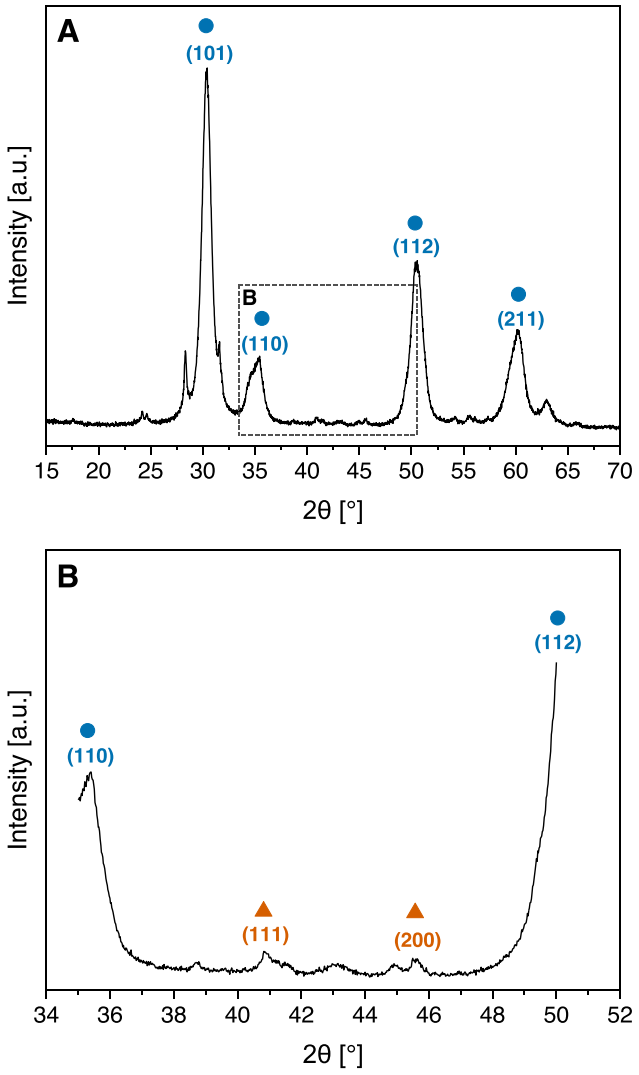

Fig. 5. XRD patterns of the Zr_Pt catalyst measured in 2θ range of 15-70° with counting time of 1 s (A) and 35-50° with counting time of 5 s (B). ZrO_2 – (●), Pt – (▲).

60.0° 2θ and indexed as (1 0 1), (1 1 0), (1 1 2) and (2 2 1) Miller indices, respectively. These crystallographic planes are typical of ZrO_2 crystallized in the tetragonal P42/nmc space group [JCPDS 79–1764]. At the calcination temperature below 1000 °C, a more stable monoclinic ZrO_2 crystallographic phase is usually formed [33]. The formation of the tetragonal ZrO_2 phase is explained by the presence of SiO_2 residues, which exist in the material after incomplete dissolution of the silica template with NaOH. This supposition was confirmed by XRF analysis, which showed the Si content of 2.1 wt%. A similar effect of ZrO_2 tetragonal form formation caused by various additives, e.g. Y, Ca, Ce, Si, La was reported [34]. The XRD measurement was repeated with a prolonged counting time per step (5 s) in a 2θ region where diffraction peaks related to the Pt active phase are expected (Fig. 5B). The (1 1 1) and (2 0 0) reflections corresponding to metallic platinum crystallographic phase are distinguished more precisely at 41.0° and 45.5 °2θ [ICDD, PDF No. 00–004–0802].

The XRF analysis revealed the bulk Pt content of 0.66 wt% in the Zr_Pt catalyst. Furthermore, the XPS measurements gave more detailed information on the form of Zr- and Pt-containing surface species. In the XPS survey spectrum (not shown), the emission of photoelectrons was observed, which confirmed the presence of Pt, Zr, O, C, Si and Na on the Zr_Pt surface. The appearance of Na 1s and Si 2p peaks should be assigned to an incomplete removal of silica from the template structure and a possible formation of sodium silicate residues [35]. This claim is in accordance with the XRF results. The Zr 3d core-level XPS spectrum (Fig. 6A) shows a spin–orbit doublet at 182.4 eV ($3d_{5/2}$) and 184.7 eV ($3d_{7/2}$) with an energy gap of 2.3 eV, which corresponds to Zr^{4+} in ZrO_2 [36]. In turn, the presence of metallic Pt is approved by well-separated spin–orbit asymmetric components of Pt $4f_{7/2}$ and Pt $4f_{5/2}$ at 71.1 eV and 74.4 eV, respectively (Fig. 6B) [37].

SEM measurements were performed to investigate morphology of the SiO_2 template as well as the corresponding C_SPH and Zr_Pt samples. The intended spherical structure of the synthesized materials is related with the concept of minimizing potential influence of grain morphology

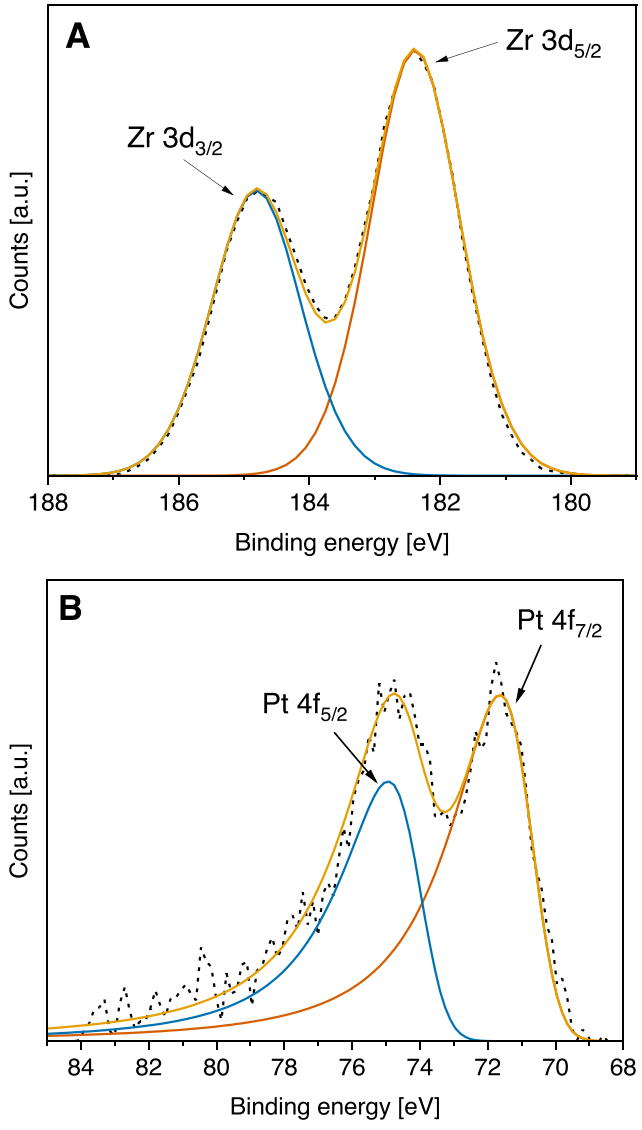

Fig. 6. XPS core level spectra of Zr 3d (A) and Pt 4f (B) regions for the Zr_Pt catalyst.

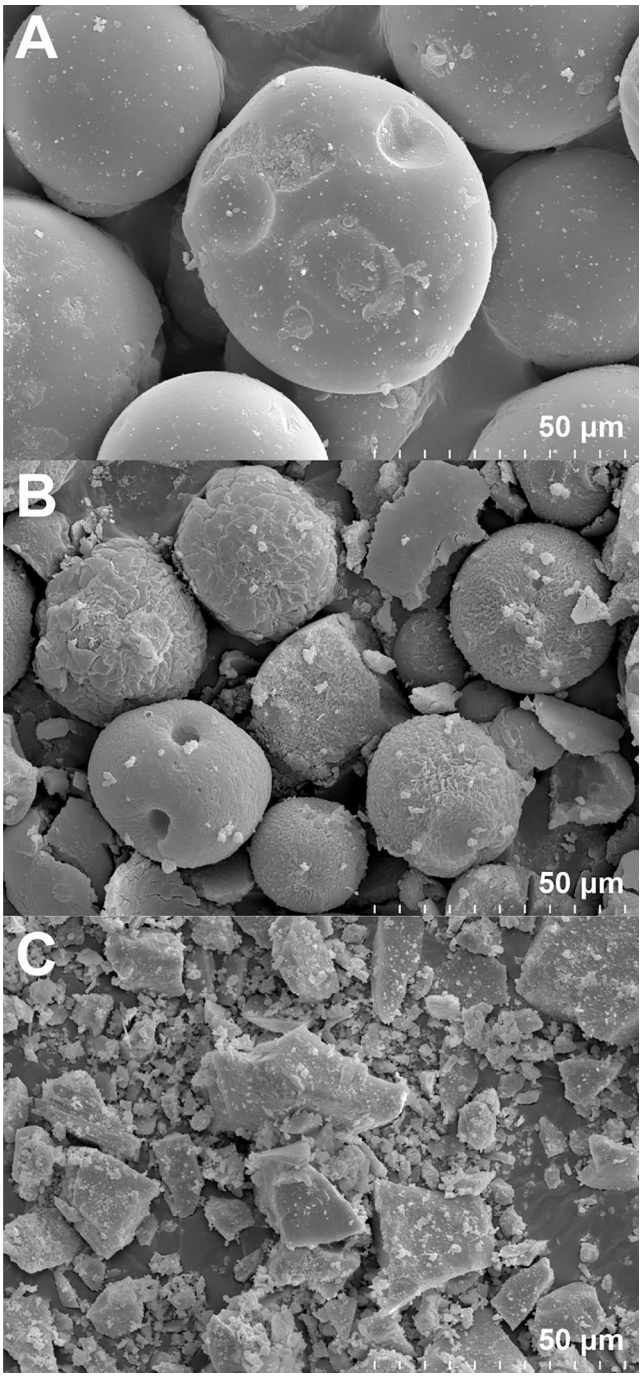

Fig. 7. SEM pictures of SPH silica (A), C_SPH carbon replica (B), and Zr_Pt catalyst (C).

of the dual-functional system components on diffusion of gas molecules. The SEM image of SPH (Fig. 7A) reveals quite regular, spherical shape of particles with a diameter of ca. 60 μm. The C_SPH carbon particles obtained by the nanoreplication method are slightly less spherical (Fig. 7B). Some of them are partially cracked with visible macrodefects and rough surface. Moreover, diameter of the replicated SPH spheres decreased to ca. 30 μm or less. Such effect is typical of sucrose-based carbon nanoreplicas. Similar outcome was reported earlier for CMK-3 type carbon, where distinct shrinkage of a structure was observed after carbonization process [38]. The nanoreplication quality was the weakest for the ZrO_2 support. The SEM picture of the Zr_Pt sample (Fig. 7C) clearly shows that the spherical structure has not been preserved after all synthesis steps, which corresponds with a broad peak observed in pore size distribution (cf. Fig. 4B). The synthesis of inorganic nanoreplicas is usually more problematic than carbon ones, due to difficulties in penetration of pores with a liquid precursor as well as effects of its thermal decomposition. Similar observations have already been reported for MgO nanoreplica – using of a CMK-3 carbon template resulted only in partial replication even at optimized conditions [39]. Nevertheless, in spite of low sphericity, the Zr_Pt catalyst exhibits a relatively high specific surface area and sufficient porosity, which allow to use it as catalyst in the next stages of the presented study. The SEM/EDS mapping was performed to determine dispersion of Pt, Zr and O elements in Zr_Pt (Fig. 8). High dispersion of all elements is observed with no local aggregation of platinum active phase. Furthermore, a temperature-programmed desorption of NH_3 measurement for the Zr_Pt catalyst showed a relatively low total surface concentration of acid sites (10.2 μmol/g_{cat}).

3.2. Performance of adsorption-catalytic system

Adsorption capacity of toluene was determined individually for all three components of multilayer adsorption-catalytic system after removing physically bound VOC molecules. The results summarized in Table 1 indicate that no noticeable traces of toluene remained on the surface of the SPH and Zr_Pt samples prior to the final thermal desorption step. It can be therefore assumed that these two components do not contribute to the overall toluene adsorption capacity of the multilayer bed. As intended, only C_SPH exhibited the relatively high adsorption capacity of toluene (8.31 mmol/g). The adsorption test was repeated over the same sample. A very similar value of adsorption capacity was reached during the second adsorption/desorption run, confirming stability of the developed adsorbent.

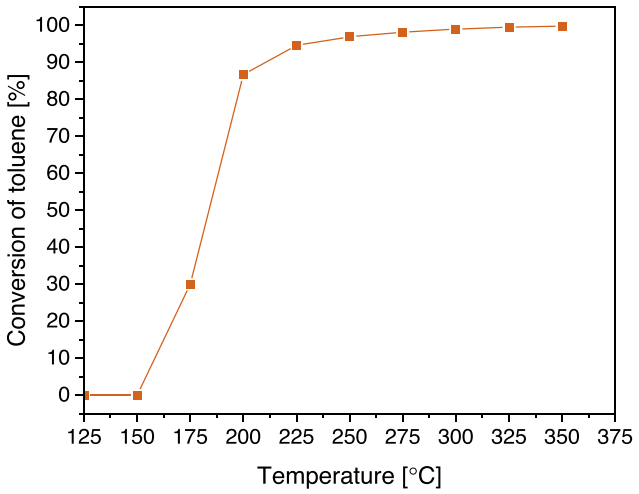

Fig. 9. Conversion of toluene with increasing reaction temperature over the Zr_Pt catalyst.

Catalytic performance of the Zr_Pt catalyst was examined to determine the optimal operating temperature, which ensures total toluene conversion in the designed multilayer system. As can be seen in Fig. 9, toluene combustion over Zr_Pt begins at 150 °C and achieves 90% conversion (T_{90}) at 210 °C. To obtain the highest possible catalytic performance in the combined adsorption-catalytic system, the temperature of 250 °C (giving more than 97.0% of toluene conversion) was selected. On the other hand, the chosen temperature is low enough to preserve the carbon adsorbent from undesirable oxidation which is very likely in the oxygen rich reaction environment.

After the thorough characterization of all individual components of the adsorption-catalytic system, adsorption followed by immediate total oxidation of desorbed toluene was tested. These experiments involving a multilayer bed are denoted as *a_s_c*, where *a* – mass of C_SPH adsorbent [mg], *s* – mass of SPH separator [mg], *c* – mass of Zr_Pt catalyst [mg]. Firstly, a double layer bed consisting of 10 mg of the C_SPH adsorbent and 50 mg of the Zr_Pt catalyst (indicated as 10_0_50) was examined.

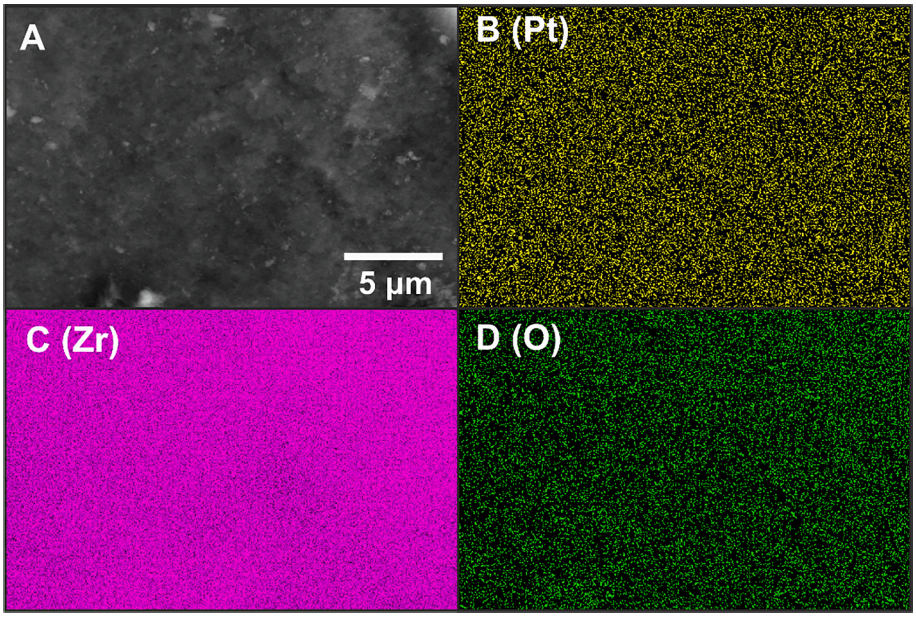

Fig. 8. SEM picture (A) and SEM/EDS elemental maps of Pt (B), Zr (C) and O (D) collected for the Zr_Pt sample.

Table 2
Conversion of toluene and mass loss of C_SPH part for the adsorbent-catalyst bed with different contents of the SPH separator.

Experiment name	Mass of SPH separator [mg]	Conversion of toluene [%]	Mass drop [%]
10_0_50	0	97.6	29.0
10_200_50	200	97.9	2.0
10_400_50	400	98.3	2.1

The conversion of toluene reached 97.6%, thus almost entire chemically adsorbed toluene was oxidized. We also noticed that the bed mass after such run decreased significantly. Taking into account the chemical nature of the bed components, only C_SPH carbon could be lost due to burning by oxygen present in air. However, this process requires temperatures higher than 250 °C (cf. Fig. 3). In that case, the necessary heat energy was most probably generated locally by the exothermic reaction of toluene combustion, quite intensive at the beginning of the process. The reaction took place on the surface of the Zr_Pt catalyst, which in this peculiar adsorbent/catalyst bed configuration was in close contact with C_SPH, where the heat flux might be easily transferred. In order to exclude that effect, the adsorption-catalytic tests with an additional protective layer of SPH were performed. Two distinct volumes of this component were used, i.e. 200 mg (10_200_50) and 400 mg (10_400_50). The SiO_2 separator was placed between exactly the same amounts of the C_SPH adsorbent (10 mg) and the Zr_Pt catalyst (50 mg). The results presented in Table 2 confirm that a negligible mass drop (~2.0 %) was detected after the runs with the bed containing the inert separator. A slightly higher conversion of toluene was also observed, up to 98.3% (+0.7%) for 10_400_50. Thus, the implementation of the SPH separator successfully protects the C_SPH carbon adsorbent from the unwanted oxidation. Moreover, this additional layer may play a supporting role of buffer space, which preserves desorbed toluene molecules present within the adsorbent bed (air flow stopped) from diffusion towards the catalyst bed before the temperature of Zr_Pt reaches the operation level of 250 °C. Such hypothetical situation may happen, when a larger amount of adsorbent is used and consequently, more toluene desorbs in a time unit and moves towards an open end of reactor. For the following measurements, 200 mg of SPH was selected as optimal, since no significant changes in the mass drop and conversion of toluene was found in the experiment involving 400 mg of SPH.

In the next stage, the catalytic efficiency of Zr_Pt was investigated to determine how much of toluene could convert under such conditions. The amounts of SPH (200 mg) and Zr_Pt (50 mg) were fixed, whereas the C_SPH mass was changed (20 mg or 40 mg), providing different amounts of toluene dosed into the catalyst layer during the thermal desorption. The obtained results are presented in Fig. 10. A slight decrease in the conversion of toluene from 97.9% for 10_200_50 to 96.7% for 20_200_50 was noticed. Thus, 50 mg of the catalyst can simply oxidize twice as much of toluene. A further increase in the adsorbent content (up to 40 mg) gave a more distinct drop of toluene conversion to 86.1%. Evidently, the 40_200_50 adsorption-catalytic system works insufficiently at such conditions.

In order to optimize the amount of catalyst, which would be adequate to restore the level of toluene conversion to that observed for 20_200_50, an additional experiment (40_200_100) with amounts of the C_SPH, SPH and Zr_Pt components fixed at 40, 200 and 100 mg, respectively, was performed. Twice the weight of the Zr_Pt catalyst resulted in the toluene conversion of 89.4%, thus lower than expected and obtained for the 20_200_50 experiment (cf. Fig. 10). Therefore, one more test was carried out with triple quantity of Zr_Pt (40_200_150). The toluene conversion reached 94.5% and was comparable to the previously observed during the 20_200_50 experiment. Concluding, for the same conversion of toluene, the mass of catalyst had to be tripled.

The optimal mass ratios of Zr_Pt to C_SPH were calculated for the experiments where the comparable toluene conversion was achieved,

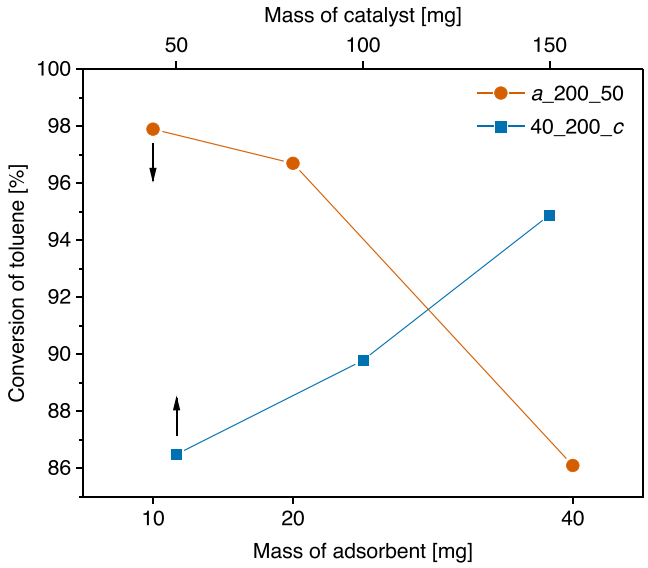

Fig. 10. Conversion of toluene for the series of experiments *a*_200_50 where *a* is mass of the C_SPH adsorbent, and 40_200_*c* where *c* is mass of the Zr_Pt catalyst.

but differed in the amount of adsorbent and catalyst layers. For the 20_200_50 and 40_200_150 tests, the ratios were equal to 2.50 mg and 3.75 mg of Zr_Pt per 1.00 mg of C_SPH, respectively. The Zr_Pt mass required to complete oxidation of desorbed toluene increases out of proportion to the amount of C_SPH. Evidently, in this kind of multilayer adsorption-catalytic systems, straightforward upscaling in order to simply increase the overall performance of the system is possible, but complex and challenging. The specific conditions may play a crucial role, including external and/or internal diffusion limitation. Moreover, utilization of carbon materials with a large specific surface area is of fundamental significance. On the one hand, as high as possible adsorption capacity, which is favourited by a high surface area, is desirable. On the other hand, volume of desorbing VOCs molecules is relatively high in comparison to physical dimensions of a reactor. Taking into account the mass of the adsorbent (40 mg) and its adsorption capacity towards toluene (8.31 mmol/g), the approximate volume of a liberated gas (at standard temperature and pressure) is equal to ca. 7.5 cm^3. That volume of toluene is a dozen times greater than the void space inside and over the separator-adsorbent layers in the reactor. The reactor void space that is clearly insufficient to contain the liberated gas could generally lead to the situation in which a part of toluene molecules would pass through the catalyst bed, before the temperature in the reactor reaches the operation level. In our case such effect was not observed, since the conversion level was quite high. In fact, the kinetics of desorption is slow enough to prevent too fast release of the adsorbed toluene molecules. Most probably, firstly desorbed toluene molecules located inside the C_SPH pores inhibit further desorption because of increased partial pressure of toluene vapour. The impeded desorption of toluene corresponds with the hysteresis observed during the N_2 adsorption–desorption measurements (cf. Fig. 4A), which usually indicates pores with nonuniform diameters responsible for such effect.

For the most efficient 40_200_150 adsorption-catalytic system for the removal of toluene, five consecutive runs were performed in order to verify its stability (Fig. 11). The relatively high stability was maintained for all experiments. A slight increase in the toluene conversion from 94.0% to 95.8% was noticed for runs 4 and 5 in contrast with matching levels of runs 1–3. The difference lies within the uncertainty range of 94.2 ± 2.1% estimated for runs 1–3, thus turned out to be negligible. Moreover, none of mass loss was observed after the sequence of adsorption/catalysis tests. It can therefore be concluded that both adsorption capacity of C_SPH and catalytic activity of Zr_Pt layers are

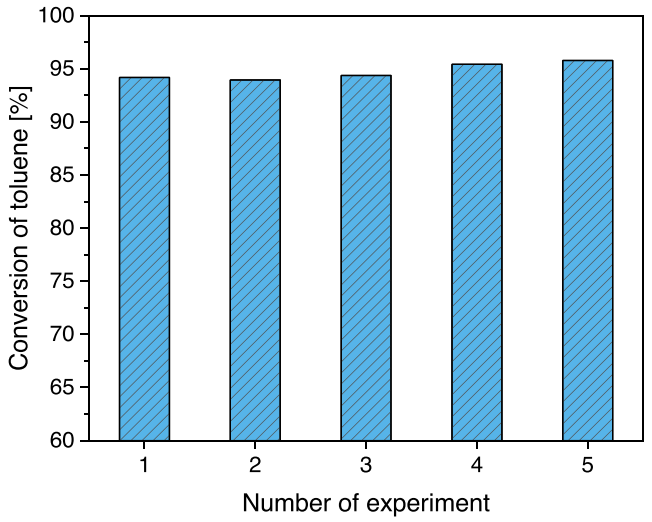

Fig. 11. Conversion of toluene for the optimal 40_200_150 adsorption-catalytic system observed in five consecutive runs.

stable enough to work in repeated cycles.

The above discussed experimental procedure involved desorption of physisorbed toluene molecules in order to precisely control the amount of toluene adsorbed on C_SPH before the catalytic combustion. However, to simulate more practical and environmental-effective conditions, the performance of the 40_200_150 system was tested for all forms of toluene adsorbed on the surface of 40 mg of C_SPH until the breakthrough of the multilayer bed. One should take into consideration that physisorption of toluene molecules is not as predictable and repeatable as chemisorption, since adsorbate multilayers can be easily formed. In the discussed experiment, after the complete saturation of C_SPH with toluene (when the breakthrough of the toluene signal appeared), the flash heating up to 250 °C started immediately, followed by the same oxidation procedure as described earlier. The adsorption capacity of physically adsorbed toluene (taking into account the value calculated from the experiment performed in pure nitrogen) was at the level of 38.23 mmol/g, therefore ca. 4.6 times greater than chemisorbed one. The conversion reached 39.3%, which gave the total amount of oxidized toluene ca. 1.9 times more (per one cycle) than in the case of chemisorption. It is apparent that the majority of the adsorbed toluene was not oxidized, most probably because of oxygen deficit and/or an insufficient amount of the catalyst.

3.3. Evaluation of energy requirement of adsorption-catalytic system

Given that the main drawback of thermal desorption is its rather long duration and thus relatively low energetic efficiency, the net energy requirement to operate the adsorption-catalytic system under isothermal conditions was evaluated. The energetic performance of the proposed hybrid system was compared with a conventional system, i.e. a catalytic flow reactor converting toluene in a continuous mode and with a constant but low feed concentration (1000 ppm), typical for such apparatuses. The key parameters used in the calculations are given in Table 3. Only the part of the quartz reactor actually loaded with the particles was taken into account in calculating the energy necessary to heat the apparatus walls. Its mass was determined on the basis of the inner and outer diameters, i.e. d_{in} and d_{out}, and lengths of individual zones, derived from the bed mass and porosity. The values of the net energy requirement determined for both systems are summarized in Table 4. The conventional continuous flow system is indicated by: (*a*)_0_*c*, where *c* denotes mass of the catalyst in mg, while *a* in round brackets indicates that the contribution of Q_{gas} to Q_{net} was determined based on such an amount of toluene that is adsorbed in the multilayer system, respectively, on 10, 20 or 40 mg of C_SPH in the multilayer bed. Keeping in mind that the conventional monolayer catalytic bed is fed continuously with the stream of air saturated with 1000 ppm of toluene and supplied at 100 cm^3/min, the duration of the process, and hence that time of gas preheating was set, respectively, to 1220, 2440 and 4880 s.

Table 3
Properties of solids and reactor used in energetic calculations and dynamic simulations.

Parameter	Value	Parameter	Value
$c_{p,wall}$	964 J/(kg·K)	ε_{p,C_SPH}	0.7879
c_{p,C_SPH}	1000 J/(kg·K)	$\varepsilon_{p,SPH}$	0.6759
$c_{p,SPH}$	1100 J/(kg·K)	ε_{p,Zr_Pt}	0.4773
c_{p,Zr_Pt}	517 J/(kg·K)	ρ_{app,C_SPH}	269.8 kg/m^3
d_{in}	8 mm	$\rho_{app,SPH}$	814.3 kg/m^3
d_{out}	10 mm	ρ_{app,Zr_Pt}	2983.3 kg/m^3
ε_b	0.4		

Table 4
Net energy requirement to operate the catalytic bed and the adsorbent-catalyst bed with different contents of the SPH separator during toluene combustion.

Experiment name	$Q_{preheat}$ [J]	Q_{gas} [J]	Q_{des} [J]	Q_{reac} [J]	Q_{net} [J]
(10)_0_50	13.31	554.12	–	–301.60	265.83
10_200_50	194.16	135.77	7.06	–306.61	30.38
10_400_50	353.53	135.77	7.06	–307.86	188.50
(20)_0_50	13.31	1108.23	–	–603.20	518.34
20_200_50	215.64	135.77	14.13	–605.70	–240.16
(40)_0_50	13.31	2216.47	–	–1206.40	1023.38
40_200_50	258.60	135.77	28.25	–1078.61	–655.99
(40)_0_100	26.63	2216.47	–	–1213.91	1029.19
40_200_100	271.91	135.77	28.25	–1119.95	–684.02

The process duration for the multilayer system was estimated based on the desorption of toluene from C_SPH determined at 250 °C in N_2 (10 cm^3/min). It was then assumed that the total oxidation can be interrupted when 99% of toluene is desorbed from C_SPH, which yields the process duration in the adsorption-catalytic system equal to 3000 s. The estimated process duration is independent of the mass of C_SPH used, and is in a perfect agreement with the experimental observations. During the measurements the total conversion of toluene was observed approximately after 2500–3300 s from the start of air supply. The energy requirement for the system preheating ($Q_{preheat}$) was evaluated as the heat necessary to increase the temperature of reactor walls, bed material and adsorbate from 25 °C to 250 °C. For the adsorption-catalytic system Q_{des} contribution was estimated assuming a typical value of the heat of desorption of toluene from activated carbon, that is 85 kJ/mol [40,41]. Note that the accepted value is more than twice greater than the heat of toluene vaporization, which is in line with a chemical nature of the analyzed adsorption–desorption process. The heat released upon the chemical reaction Q_{reac} was calculated as the product of the actually oxidized amount of toluene and the heat of reaction evaluated at 250 °C (ΔH_{reac} = –3768.79 kJ/mol).

For the flow system (Table 4), due to negligible contribution of $Q_{preheat}$ term to Q_{net}, comparable values of X_{VOC} obtained experimentally with 50 mg and 100 mg of Zr_Pt (96.3% and 97.0%, respectively) and Q_{gas} term being always around twice greater than Q_{reac} (with the opposite sign), the obtained net energy consumption is practically proportional to the amount of toluene supplied to the reactor. The specific heat consumption for the cases evaluated here varies from 3078.76 J/mmol (for (40)_0_100) to 3198.97 J/mmol (for (10)_0_50) of toluene.

The overall energy requirements obtained for the multilayer adsorption-catalytic system are quite surprising. It turns out that for most arrangements (i.e. 20_200_50, 40_200_50 and 40_200_100) a substantial amount of heat is generated by the system. It must be recalled that the heat losses were neglected in the evaluation of energy requirement. However, considering that the process duration in the

multilayer bed was estimated to be 3000 s, that is much shorter than in the cases indicated by (40)_0_50 and (40)_0_100 (4880 s), and only slightly longer than for (20)_0_50 (2440 s), a substantial energetic superiority of the hybrid system over the flow reactor is unquestionable. As a result of a significant contribution of the SPH separator to $Q_{preheat}$ and more diverse performance of the adsorption-catalytic system in terms of conversion (varying from 86.1% for 40_200_50 to 98.4% for 10_400_50), there is no straightforward relationship between the specific multilayer arrangements in terms of Q_{net}. The arrangements that perform best, in terms of specific net heat, are 40_200_50 and 40_200_100 with the heat released by the system being equal, respectively to −1973.49 and −2057.82 J/mmol. However, it must be reminded that these arrangements are characterized by the lowest conversion of toluene. Therefore, the choice of optimal system – in terms of energy – definitely has to go in pair with the choice of the system that is also optimal in terms of the efficiency in VOCs processing. Here, this is the 20_200_50 system, for which the estimated specific net energy released is −1445.00 J/mmol of toluene desorbed from C_SPH.

3.4. Transient behavior of adsorption-catalytic system

The experimental results for the adsorption-catalytic system and evaluation of its energetic requirements clearly indicate that the overall performance is strictly related to the transient character of the process and, to different time scales of the physical and chemical phenomena. A relatively high amount of heat released during the total oxidation of toluene in the hybrid system may suggest that the system could be operated autothermally. However, in a contrast to the flow system, the rate of supply of toluene to Zr_Pt layer strongly depends on the desorption rate that varies in time. Thus, especially in the final stages, when the gas phase concentration of toluene is very low, the heat of combustion is insufficient to sustain the process. Different time scales, i.e. variable kinetics of desorption combined with relatively low residence time of gas in each layer and very rapid catalytic reaction, determine in turns the overall dynamics of the process.

Fig. 12 shows temporal evolution of the concentration of toluene $q(t)$ in the C_SPH layer during its desorption from the adsorbent surface. The experimental curve was derived based on the desorption tests performed at 250 °C in N_2 and was approximated using Eq. (14). Additionally, the gas phase molar fraction curves of toluene $y_{VOC,1}(t)$ in the C_SPH layer are plotted. They were determined for three values of the adsorbent mass employed in the experiments, i.e. 10, 20 and 40 mg, using the model for C_SPH zone only, i.e. Eq. (9), resolved in the MATLAB software with the aid of ode15s solver. The physical properties appearing in the model are reported in Table 3.

While initially the solid phase concentration of toluene q drops quite rapidly, a complete desorption of toluene molecules from the C_SPH surface requires, as already mentioned, more than 3000 s. Another important issue, from the point of view of efficient operation of the hybrid system, is the peak molar fraction of toluene in gas phase $y_{VOC,1}$ that reaches values of 0.0252, 0.0492 and 0.0938, respectively for 10, 20 and 40 mg of C_SPH. Considering the combustion of toluene:

$$C_7H_8 + 9O_2 \rightarrow 7CO_2 + 4H_2O \quad (16)$$

an oxygen deficiency might be encountered in the Zr_Pt zone in the interval characterized by the highest rate of desorption, and thus the highest rate of supply of combustible from the C_SPH to the Zr_Pt layer. This observation explains the poorer performance, in terms of conversion, of the adsorption-catalytic system operated with 40 mg of the adsorbent.

Fig. 13A shows representative oxygen and toluene molar fraction curves used to derive the kinetic equation for toluene combustion in the hybrid system. They were registered at the reactor outlet during a test performed using the arrangement labeled as 20_200_50. The location of the toluene peak and the corresponding minimum of oxygen concentration is quite surprising since the maximum molar fraction of toluene in the gas stream leaving the Zr_Pt layer is observed around 40 s after the start of air supply. On the other hand, the highest rate of toluene supply from C_SPH to the Zr_Pt layer predicted using the empirical model of desorption (Fig. 12) is observed slightly later, i.e. ~ 3 min. The toluene molar fraction at the reactor outlet $y_{VOC,3}(t)$ (Fig. 13A) suggests that it is the effect of a much faster desorption process than expected. Note that the desorption rate was determined based on desorption tests performed at 250 °C in N_2. Although the system temperature was also maintained at 250 °C during the combustion experiments, as already mentioned, the

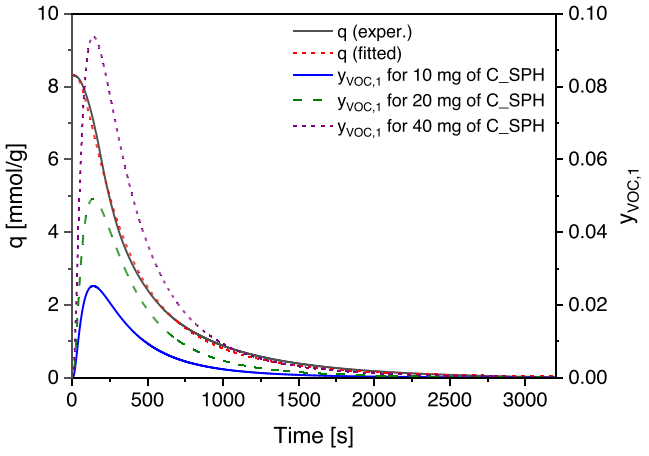

Fig. 12. Temporal evolution of the concentration of toluene in gas and solid phases in the C_SPH layer.

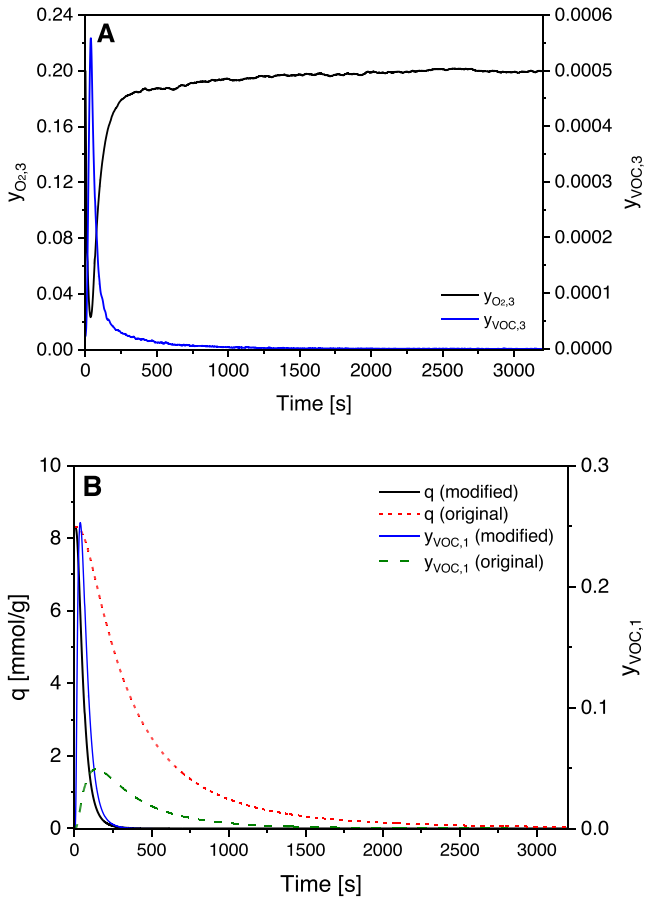

Fig. 13. Measured concentration of oxygen and toluene at the outlet of Zr_Pt layer (A) and modified toluene concentration curves in gas and solid phases of C_SPH layer (B) for 20_200_50 system.

heat generated locally in the Zr_Pt layer can be dissipated towards the separator, and also towards the adsorbent. This in effect enhances the desorption rate, especially at the beginning of the process when the thermal energy generation rate is very high. Therefore, prior to determination of the combustion rate, the parameters of desorption model were modified to follow the peak of unconverted toluene by imposing a fixed peak location within the fitting procedure. Fig. 13B shows a comparison of $q(t)$ and $y_{VOC,1}(t)$ curves determined for 20 mg of C_SPH before ($\mu = 5.749$ and $\sigma = 0.892$) and after modification of μ and σ ($\mu_{org} = 4.024$ and $\sigma_{org} = 0.625$).

The above observation about the effect of thermal energy released during the toluene combustion on the desorption dynamics from C_SPH also indicates an additional role of the SPH separator. It can thus be argued that separating the desorption layer from the reaction (catalytic) layer not only protects C_SPH from unwanted oxidation, but also allows to control more easily the desorption process and thus the rate of toluene supply to the catalytic layer. The larger the separator, the easier it is to avoid overheating of C_SPH at the initial stage of the process and, consequently, too high a rate of desorption leading to oxygen deficiency in the Zr_Pt bed and, as a result, lower system performance.

A qualitative prediction of the dynamic behavior of the system with respect to changes in the geometrical properties of the system is shown in Fig. 14. Since less severe conditions from the point of view of oxygen consumption were used as a reference (system labeled as 20_200_50), the first-order kinetic equation with respect to toluene, i.e. $r_{VOC} = k_{app}C_{VOC}$ turned out to fit the experimental data much better than the more elaborate formula (e.g. Eq. (15)). The value of the determined apparent rate constant is $k_{app} = 7.357 \cdot 10^3$ 1/s. Fig. 14A shows the prediction of the dynamics of the hybrid system when the mass of C_SPH is varied, the reference being 20 mg, while the results obtained when the mass of SPH is varied are shown in Fig. 14B. For the reference conditions, i.e. the arrangement 20_200_50, the predicted molar fraction of toluene at the outlet of Zr_Pt, $y_{VOC,3}(t)$, is additionally compared with the experimental result (dotted line). Due to the complexity of the process, the peak value of the molar fraction of toluene at the outlet determined from the model is slightly underestimated. Furthermore, it can be observed in Fig. 14A that the experimental curve has a much heavier tail than the calculated one. The inflection of the experimental curve $y_{VOC,3}(t)$, which can be observed ~ 100 s, suggests a change in the desorption kinetics from C_SPH, which may be due to the temperature effect or due to near-equilibrium conditions. From a qualitative point of view, a decrease and an increase in the mass of C_SPH (with the mass of SPH and Zr_Pt unchanged) lead to a decrease and an increase in the outlet toluene concentration, respectively (Fig. 14A). The effect of the change in SPH mass is much less pronounced here (Fig. 14B). The separator primarily plays a lagging role in the delivery of toluene from C_SPH to the Zr_Pt layer. This is reflected in a slight shift of the peak positions of $y_{VOC,3}(t)$ in time. Furthermore, due to the additional volume added to the system, this leads to a reduction in the toluene concentration delivered to the Zr_Pt layer, which in turn results in slightly lower peak values at the reactor outlet.

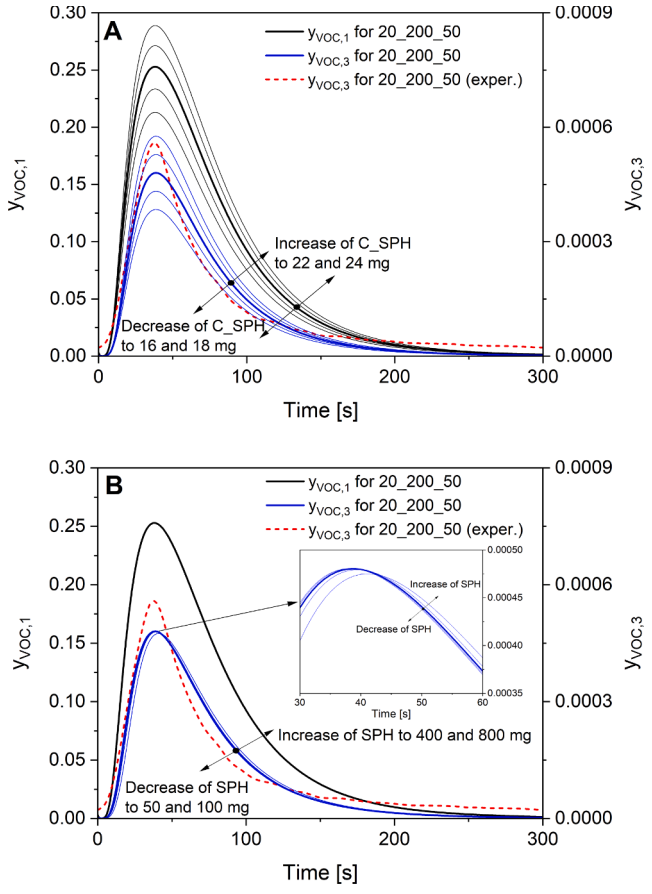

Fig. 14. Influence of geometric modifications of the hybrid system onto toluene concentration in gas phase of C_SPH and at the reactor outlet.

4. Conclusions

Porous carbon adsorbent and ZrO_2 support were synthesized by nanoreplication using commercial spherical silica as a template and sucrose or $ZrOCl_2 \cdot 8H_2O$ as final material precursors, respectively. The Pt active phase (0.66 wt%) was incorporated with the polyol process using $PtCl_4$ and ethylene glycol. Characterization techniques (including TGA, low-temperature adsorption of N_2, XRD, XPS, SEM-EDS) revealed that both active constituents of a dual-functional adsorptive-catalytic system exhibited desirable physical and chemical properties, such as relatively high specific surface area, tetragonal crystallographic structure of the ZrO_2 support and high dispersion of metallic Pt active phase. The performance of the multilayer bed consisting of carbon adsorbent, silica separator and Pt/ZrO_2 catalyst was optimized. It was shown that the presence of the inert silica separator was required to prevent the carbon adsorbent from partial oxidation induced by heat of exothermic toluene oxidation in the catalyst bed. An influence of the mass ratio of catalyst to carbon adsorbent on the effectiveness of the combined system was studied. Interestingly, the Pt/ZrO_2 catalyst mass required to completely oxidize of desorbed toluene increased out of proportion to the amount of carbon adsorbent. The detailed considerations of adsorption capacity and dimensions of a reactor and layers showed that the amount of toluene to be liberated from the adsorbent, influenced by diffusion, played a crucial role. Finally, the repeated adsorption–desorption-oxidation cycles confirmed stability of the developed system, which could work with constant efficiency and with no noticeable drop in the carbon adsorbent mass.

Assessment of the energetic performance of the multilayer bed proved that the developed hybrid system is not only superior, in terms of the energy input required to sustain the combustion of toluene to the traditional catalytic reactor, but for an appropriately chosen mass ratio of adsorbent and catalyst a substantial amount of heat is generated within the system. However, considering the dynamic nature of the desorption process, the autothermal operation of the dual-functional adsorptive-catalytic system seems to be very challenging. Indeed, as shown by analysing the concentration of toluene in the C_SPH layer during thermal desorption and calculations performed using a simplified mathematical model of the hybrid system, the VOCs concentration in the gas phase is relatively high only during the first few minutes of the desorption-reaction process, while its completion requires hours.

The toluene peak in the adsorbent layer appears to be further enhanced by heat transport from the catalytic zone towards the adsorbent. This effect can be compensated by selecting a separator with sufficient volume. As shown in this study using an isothermal model, from a

mass balance point of view, the separator has mainly a retarding role in mass transport from C_SPH to Zr_Pt. However, one has to keep in mind that thorough optimization of the protective layer of SPH may not only prevent partial burning of C_SPH, encountered during experimental tests, but also may help control more easily the desorption process and thus the rate of toluene supply to the catalytic layer. This, in turn, can prevent the risk of oxygen deficiency resulting from too rapid an inflow of VOCs towards the catalyst bed. Despite significant simplifying assumptions of the formulated mathematical model, the combination of the results of numerical simulations of qualitative nature with the results of experimental studies and energetic analysis enabled the identification of key aspects, including directions for more complex mathematical description, to be considered in the further rigorous optimization of the proposed hybrid solution.

CRediT authorship contribution statement

Sebastian Jarczewski: Conceptualization, Methodology, Investigation, Visualization, Writing – original draft. **Katarzyna Barańska:** Investigation. **Marek Drozdek:** Investigation. **Marek Michalik:** Investigation. **Katarzyna Bizon:** Conceptualization, Methodology, Investigation, Visualization, Writing – original draft, Writing – review & editing. **Piotr Kuśtrowski:** Conceptualization, Methodology, Writing – review & editing, Supervision.

Declaration of Competing Interest

The authors declare that they have no known competing financial interests or personal relationships that could have appeared to influence the work reported in this paper.

Acknowledgements

The research has been funded from the Anthropocene Priority Research Area budget under the program “Excellence Initiative - Research University” at Jagiellonian University.

References

[1] X. Liang, X. Chen, J. Zhang, T. Shi, X. Sun, L. Fan, L. Wang, D. Ye, Reactivity-based industrial volatile organic compounds emission inventory and its implications for ozone control strategies in China, Atmos. Environ. 162 (2017) 115–126, https://doi.org/10.1016/j.atmosenv.2017.04.036.

[2] K. Zhang, L.i. Li, L. Huang, Y. Wang, J. Huo, Y. Duan, Y. Wang, Q. Fu, The impact of volatile organic compounds on ozone formation in the suburban area of Shanghai, Atmos. Environ. 232 (2020) 117511, https://doi.org/10.1016/j.atmosenv.2020.117511.

[3] E. Sher, Environmental Aspects of Air Pollution, in: E. Sher (Ed.), Handbook of Air Pollution form Internal Combustion Engines – Pollutant Formation and Control, Academic Press, San Diego, 1998, pp. 35–37, https://doi.org/10.1016/B978-0-12-639855-7.X5038-8.

[4] M. Kampa, E. Castanas, Human health effects of air pollution, Environ. Pollut. 151 (2) (2008) 362–367, https://doi.org/10.1016/j.envpol.2007.06.012.

[5] European Environment Agency, European Union emission inventory report 1990–2019, Publications Office of the European Union, Luxembourg (2021) 50–51, https://doi.org/10.2800/701303.

[6] R. Atkinson, J. Arey, Atmospheric Degradation of Volatile Organic Compounds, Chem. Rev. 103 (12) (2003) 4605–4638, https://doi.org/10.1021/cr0206420.

[7] H. Wang, L. Nie, J. Li, Y. Wang, G. Wang, J. Wang, Z. Hao, Characterization and assessment of volatile organic compounds (VOCs) emissions from typical industries, Chin. Sci. Bull. 58 (7) (2013) 724–730, https://doi.org/10.1007/s11434-012-5345-2.

[8] X. Li, L.i. Zhang, Z. Yang, P. Wang, Y. Yan, J. Ran, Adsorption materials for volatile organic compounds (VOCs) and the key factors for VOCs adsorption process: A review, Sep. Purif. Technol. 235 (2020) 116213, https://doi.org/10.1016/j.seppur.2019.116213.

[9] B. Belaissaoui, J. Claveria-Baro, A. Lorenzo-Hernando, D. Albarracin Zaidiza, E. Chabanon, C. Castel, S. Rode, D. Roizard, E. Favre, Potentialities of a dense skin hollow fiber membrane contactor for biogas purification by pressurized water absorption, J. Membr. Sci. 513 (2016) 236–249, https://doi.org/10.1016/j.memsci.2016.04.037.

[10] R. Ravi, L. Philip, T. Swaminathan, Comparison of biological reactors (biofilter, biotrickling filter andmodified RBC) for treating dichloromethane vapors, J. Chem. Technol. Biotechnol. 85 (5) (2010) 634–639, https://doi.org/10.1002/jctb.v85:510.1002/jctb.2344.

[11] C. He, J. Cheng, X. Zhang, M. Douthwaite, S. Pattisson, Z. Hao, Recent Advances in the Catalytic Oxidation of Volatile Organic Compounds: A Review Based on Pollutant Sorts and Sources, Chem. Rev. 119 (7) (2019) 4471–4568, https://doi.org/10.1021/acs.chemrev.8b0040810.1021/acs.chemrev.8b00408.s001.

[12] Z. Zhang, Z. Jiang, W. Shangguan, Low-temperature catalysis for VOCs removal in technology and application: A state-of-the-art review, Catal. Today 264 (2016) 270–278, https://doi.org/10.1016/j.cattod.2015.10.040.

[13] M. Popova, S. Boycheva, H. Lazarova, D. Zgureva, K. Lázár, Á. Szegedi, VOC oxidation and CO_2 adsorption on dual adsorption/catalytic system based on fly ash zeolites, Catal. Today 357 (2020) 518–525, https://doi.org/10.1016/j.cattod.2019.06.070.

[14] B.C. Trung, L.N.Q. Tu, L.D. Thanh, N. Van Dung, N.T. An, N.Q. Long, Combined adsorption and catalytic oxidation for low-temperature toluene removal using nano-sized noble metal supported on ceria-granular carbon, J. Environ. Chem. Eng. 8 (2) (2020) 103546, https://doi.org/10.1016/j.jece:2019.103546.

[15] A.N. Zagoruiko, V.V. Mokrinskii, S.A. Veniaminov, A.S. Noskov, On the performance stability of the MnO_x/Al_2O_3 catalyst for VOC incineration under forced adsorption-catalytic cycling conditions, J. Environ Chem. Eng. 5 (6) (2017) 5850–5856, https://doi.org/10.1016/j.jece:2017.11.019.

[16] S.V. Zazhigalov, P.E. Mikenin, S.A. Lopatin, D.V. Baranov, D.A. Pisarev, N. A. Chumakova, A.N. Zagoruiko, An improved adsorption–catalytic process for removing volatile organic compounds from exhaust gases, Catal. Ind. 8 (3) (2016) 231–241, https://doi.org/10.1134/S2070050416030144.

[17] S. Zazhigalov, P. Mikenin, D. Pisarev, D. Baranov, S. Lopatin, N. Chumakova, A. Zagoruiko, Modifications of the adsorption-catalytic system for organic impurities removal, Chem. Eng. Process. Process Intensif. 122 (2017) 538–549, https://doi.org/10.1016/j.cep.2017.04.011.

[18] S. Zazhigalov, N. Chumakova, A. Zagoruiko, Adsorption-catalytic process for removal of volatile organic compounds from lean waste gases: Optimization of the adsorbent-catalyst bed geometry, Chem. Eng. Process. Process Intensif. 132 (2018) 1–10, https://doi.org/10.1016/j.cep.2018.08.002.

[19] S.W. Baek, J.R. Kim, S.K. Ihm, Design of dual functional adsorbent/catalyst system for the control of VOC's by using metal-loaded hydrophobic Y-zeolites, Catal. Today 93–95 (2004) 575–581, https://doi.org/10.1016/j.cattod.2004.06.107.

[20] G.A. Atwood, H.L. Greene, P. Chintawar, R. Rachapudi, B. Ramachandran, C. A. Vogel, Trichloroethylene sorption and oxidation using a dual function sorbent/catalyst in a falling furnace reactor, Appl. Catal. B Environ. 18 (1-2) (1998) 51–61, https://doi.org/10.1016/S0926-3373(98)00023-X.

[21] P.S. Chintawar, H.L. Greene, Adsorption and catalytic destruction of trichloroethylene in hydrophobic zeolites, Appl. Catal. B Environ. 14 (1-2) (1997) 37–47, https://doi.org/10.1016/S0926-3373(97)00010-6.

[22] H.L. Greene, D.S. Prakash, K. v. Athota, Combined sorbent/catalyst media for destruction of halogenated VOCs, Appl. Catal. B Environ. 7 (1996) 213–224. https://doi.org/10.1016/0926-3373(95)00047-X.

[23] B.O. Adebayo, A. Krishnamurthy, A.A. Rownaghi, F. Rezaei, Toluene Abatement by Simultaneous Adsorption and Oxidation over Mixed-Metal Oxides, Ind. Eng. Chem. Res. 59 (30) (2020) 13762–13772, https://doi.org/10.1021/acs.iecr.0c0255010.1021/acs.iecr.0c02550.s001.

[24] B.O. Adebayo, K. Newport, H. Yu, A.A. Rownaghi, X. Liang, F. Rezaei, Atomic Layer Deposited $Ni/ZrO_2–SiO_2$ for Combined Capture and Oxidation of VOCs, Appl. Mater. Interfaces 12 (35) (2020) 39318–39334, https://doi.org/10.1021/acsami.0c1166610.1021/acsami.0c11666.s001.

[25] B.O. Adebayo, A. Krishnamurthy, Q. Al-Naddaf, A.A. Rownaghi, F. Rezaei, Investigation of Combined Capture-Destruction of Toluene over Pd/MIL-101 and TiO_2/MIL-101 Dual Function Materials, Energy Fuels 35 (16) (2021) 13256–13267, https://doi.org/10.1021/acs.energyfuels.1c0195010.1021/acs.energyfuels.1c01950.s001.

[26] Z.-Z. Xie, L. Wang, G. Cheng, L. Shi, Y.-B. Zhang, Adsorption properties of regenerative materials for removal of low concentration of toluene, J. Air Waste Manage. Assoc. 66 (12) (2016) 1224–1236, https://doi.org/10.1080/10962247.2016.1209257.

[27] E. Kullavanijaya, D.L. Trimm, N.W. Cant, Adsocat: Adsorption/catalytic combustion for VOC and odour control, Stud. Surf. Sci. Catal. 130 A (2000) 569–574. https://doi.org/10.1016/s0167-2991(00)81018-6.

[28] M. Guillemot, J. Mijoin, S. Mignard, P. Magnoux, Volatile organic compounds (VOCs) removal over dual functional adsorbent/catalyst system, Appl. Catal. B Environ. 75 (3-4) (2007) 249–255, https://doi.org/10.1016/j.apcatb.2007.04.020.

[29] G.-H. Xiu, T. Nitta, P. Li, G. Jin, Breakthrough Curves for Fixed-Bed Adsorbers: Quasi-Lognormal Distribution Approximation, AIChE J. 43 (4) (1997) 979–985, https://doi.org/10.1002/(ISSN)1547-590510.1002/aic.v43:410.1002/aic.690430413.

[30] M. Duplančić, V. Gomzi, A. Pintar, S. Kurajica, V. Tomašić, Experimental and theoretical (ReaxFF) study of manganese-based catalysts for low-temperature toluene oxidation, Ceram. Int. 47 (3) (2021) 3108–3121, https://doi.org/10.1016/j.ceramint.2020.09.147.

[31] C. Hu, Catalytic combustion kinetics of acetone and toluene over $Cu_{0.13}Ce_{0.87}O_y$ catalyst, Chem. Eng. J. 168 (3) (2011) 1185–1192, https://doi.org/10.1016/j.cej.2011.02.006.

[32] M. Thommes, K. Kaneko, A. v. Neimark, J.P. Olivier, F. Rodriguez-Reinoso, J. Rouquerol, K.S.W. Sing, Physisorption of gases, with special reference to the evaluation of surface area and pore size distribution (IUPAC Technical Report), Pure Appl. Chem. 87 (2015) 1051–1069. https://doi.org/10.1515/pac-2014-1117.

[33] K.V.R. Chary, G.V. Sagar, C.S. Srikanth, V.V. Rao, Characterization and catalytic functionalities of copper oxide catalysts supported on zirconia, J. Phys. Chem. B. 111 (3) (2007) 543–550, https://doi.org/10.1021/jp063335x.

[34] M. Labaki, S. Siffert, J.-F. Lamonier, E.A. Zhilinskaya, A. Aboukaïs, Total oxidation of propene and toluene in the presence of zirconia doped by copper and yttrium. Role of anionic vacancies, Appl. Catal. B Environ. 43 (3) (2003) 261–271, https://doi.org/10.1016/S0926-3373(02)00312-0.

[35] A. Mekki, D. Holland, C.F. McConville, M. Salim, An XPS study of iron sodium silicate glass surfaces, J. Non-Cryst. Solids. 208 (3) (1996) 267–276, https://doi.org/10.1016/S0022-3093(96)00523-6.

[36] A.C.Q.M. Meijers, A.M. de Jong, L.M.P. van Gruijthuijsen, J.W. Niemantsverdriet*, Preparation of zirconium oxide on silica and characterization by X-ray photoelectron spectroscopy, secondary ion mass spectrometry, temperature programmed oxidation and infra-red spectroscopy, Appl. Catal. 70 (1) (1991) 53–71, https://doi.org/10.1016/S0166-9834(00)84154-8.

[37] S. Mostafa, J.R. Croy, H. Heinrich, B.R. Cuenya, Catalytic decomposition of alcohols over size-selected Pt nanoparticles supported on ZrO_2: A study of activity, selectivity, and stability, Appl. Catal. A Gen. 366 (2) (2009) 353–362, https://doi.org/10.1016/j.apcata.2009.07.028.

[38] S. Jarczewski, M. Drozdek, P. Michorczyk, C. Cuadrado-Collados, J. Gandara-Loe, J. Silvestre-Albero, P. Kuśtrowski, Oxidative dehydrogenation of ethylbenzene over CMK-1 and CMK-3 carbon replicas with various mesopore architectures, Microporous Mesoporous Mater. 271 (2018) 262–272, https://doi.org/10.1016/j.micromeso.2018.06.007.

[39] S. Jarczewski, M. Drozdek, P. Michorczyk, C. Cuadrado-Collados, J. Gandara-Loe, J. Silvestre-Albero, L. Lityńska-Dobrzyńska, P. Kuśtrowski, On the catalytic role of superficial VO_x species and coke deposited on mesoporous MgO replica in oxidative dehydrogenation of ethylbenzene, Appl. Surf. Sci. 504 (2020) 144336, https://doi.org/10.1016/j.apsusc.2019.144336.

[40] P.J. Reucroft, D. Rivin, Gas/vapor flow microcalorimetry on porous carbons I, Heat of adsorption of toluene on a microporous carbon, Carbon. 35 (8) (1997) 1067–1071, https://doi.org/10.1016/S0008-6223(97)00061-4.

[41] T. Chafik, A. Darir, O. Achak, A.P. Carvalho, J. Pires, Determination of the heat effects involved during toluene vapor adsorption and desorption from microporous activated carbon, C.R. Chim. 15 (6) (2012) 474–481, https://doi.org/10.1016/j.crci.2012.04.001.